Applied Thermal Engineering 211 (2022) 118506

Contents lists available at ScienceDirect

Applied Thermal Engineering

journal homepage: www.elsevier.com/locate/apthermeng

Research Paper

Numerical modelling of a finless heat exchanger layout for electric vehicle application

Mattia Samiolo, Patrick G. Verdin *

Energy and Power, Cranfield University, Cranfield MK43 0AL, UK

ARTICLE INFO

Keywords:
OpenFOAM
k-omega SST
Heat exchanger
Drag coefficient

ABSTRACT

Computational Fluid Dynamics has emerged as one of the major investigative tools for aerodynamics and thermal analyses of today's road vehicle design processes. This work presents the design of a new heat exchanger layout that could support the transition from thermal to electrical propulsion of an existing motor vehicle. A procedure is established to develop and assess a heat exchanger prototype. The aerodynamic performance of an electric vehicle equipped with the above-mentioned heat exchanger is assessed numerically, and results compared with its thermal counterpart. The comparison between both layouts shows a 5% reduction of the vehicle's drag and a net reduction of the overall weight with the newly designed system, introducing the proposal for a new form of heat exchanger packaging.

1. Introduction

Research and development on hybrid electric vehicles (HEVs) and full battery electric vehicles (BEVs) have intensified over the last decade [1]. The automotive industry is renowned for its competitive environment, and the current trend is to prepare the transition from thermal to electric propulsion, with a consequent rearrangement of the line products for all traditional car manufacturers. The main industry request is to reduce costs, maintaining at the same time the wide portfolio of products created during past years, to make a profit as high as possible. The idea of maintaining the same vehicle layout for different propulsion methods is attractive. Consequently, significant efforts have been made to modify vehicles already in production and minimize the transition cost [2].

In a traditional vehicle, more than 33% of the energy generated by the engine via combustion is lost through heat [1]. Devices such as Heat Exchangers (HEs) enable the powertrain to dissipate the heat produced during the generation of motive power and avoid overheating. Automotive HEs mainly use coolant as a working fluid (water with additives, propylene glycol in most cases) to overcome the shortcomings of water as a heat transfer fluid (change of phase). Most modern cars use aluminium radiators, made by brazing thin fins to flattened tubes in a parallel arrangement. The accurate description of traditional automotive HEs given in [1], highlights the importance of the wettable surfaces and turbulent state of the working fluids. Modern-day studies are carried out to develop current HE systems, for instance through parametric studies to evaluate different HE fins' layouts and establish best practices to characterise these devices [3]. This can be achieved through evaluating the performance of flat-tube heat exchangers with louvered fins and optimise them [4], or through describing the aerodynamic impact of the fins' shape on the HE performance [5]. Computational Fluid Dynamics (CFD) techniques are highly used for this type of research, for instance, to assess and improve the performance of a HE through conjugate heat transfer [6], to evaluate the performance of a HE using a multiphase working fluid, applying an advanced treatment of the phase interfaces within a complex-shaped domain [7] and to characterise a HE by studying only a portion of the device itself [8].

A performance indicator for these devices is the effectiveness, a parameter that describes the perfect thermodynamic heat exchange with a unit value. HE's effectiveness stays around 40% for automotive utilization compared to the 90% achieved in the system engineering field [9]. Automotive HEs are built to achieve a high ratio of efficiency per unit cost, and several attempts have been made to enhance the efficiency of the heat exchange process, keeping the effectiveness/cost ratio as main target. The novel predominant methods to improve the thermal property of these devices make use of nanofluids [10], while another common strategy is through the use of advanced temperature control [11]. These methods are interesting as they do not include radical layout modifications; established HE layouts (produced in the order of millions of units) have optimised costs to such an extent that the creation of new

* Corresponding author.
E-mail addresses: mattia.samiolo@cranfield.ac.uk (M. Samiolo), p.verdin@cranfield.ac.uk (P.G. Verdin).

https://doi.org/10.1016/j.applthermaleng.2022.118506
Received 18 December 2021; Received in revised form 12 March 2022; Accepted 8 April 2022
Available online 11 April 2022
1359-4311/© 2022 The Author(s). Published by Elsevier Ltd. This is an open access article under the CC BY license (http://creativecommons.org/licenses/by/4.0/).

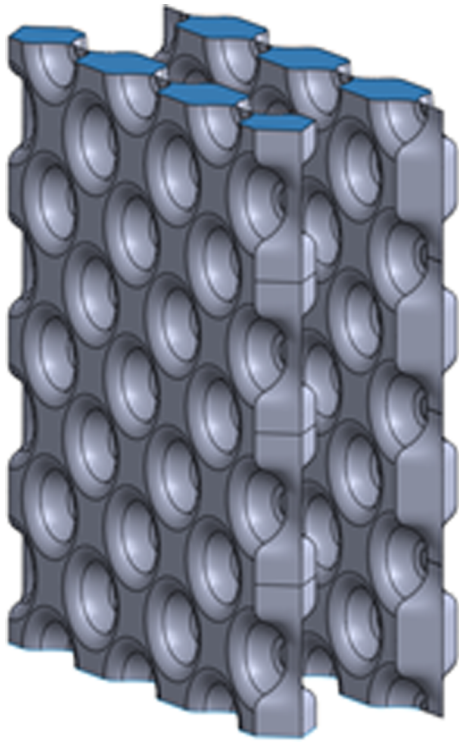


Fig. 1. Heat Exchanger portion.

layouts becomes complex [1].

However, as far as the thermal management of a vehicle is concerned, the switch to electric propulsion brings several advantages. Chief among them is the need to dissipate relatively low power. This need for heat to be dissipated in Electric Vehicles (EV) might make the well-established devices unfit, due to other prioritized characteristics from design requirements. Lower effectiveness requirements allow the main focus to be diverted from the enhancement of efficiency of the HE itself to other characteristics such as cost, aerodynamic efficiency, lightness and packaging opportunities. The aim of this work is to provide an innovative solution for vehicle HEs to lead the thermal/electric transition, providing an innovative HE layout to substitute/pair the traditional units.

Traditional mechanisms to transfer heat in automotive HEs introduce complications in the design, such as fins and tanks. To supplant those widespread and established traditional HE layouts, any novel design must be lower in cost, even in the first phase of the design, to show the feasibility for line production. A lower cost per unit can be obtained if a mechanism to exchange heat is found to reduce the complexity of the existing devices without altering the positive characteristics already in place. Consequently, to subject the device to new design criteria, HEs must be re-designed and positioned adequately for future applications of electric powertrains. The present research is applied to an industrial case, presenting a HE layout for a specific vehicle (sports car).

To correctly reproduce the condition of movement of a vehicle, significant experimental effort is required. The detailed visualization of the flow structures, which is indispensable for the overall understanding of the dynamics of a car, is often challenging when running experiments [12]. CFD has thus become increasingly important in the automotive development process as it offers the opportunity to visualize flow structures and model the moving ground with a minimum effort, even if numerical results will still need to be validated against experimental data. *OpenFOAM® v2012* has been used to perform both the pre-processing and the numerical calculation. In past studies, this software has shown good agreement with experimental data when predicting the aerodynamic features of automobiles [12]. The related post-processing tasks have been carried out with *ParaView 5.9.1*. The mesh has been generated with *snappyHexMesh*, a native mesh builder of the OpenFOAM® suite. Note that, the use of the software has been facilitated through the corresponding OpenFOAM® Technology primer [13].

2. Heat exchanger design

Inspiration for this work has been taken from the shell layout described in [14], which increases the turbulent phenomena in a HE layout characterised by a dimpled pattern, and thus enhances the thermal performance. The use of dimples is not new in itself. Dimples have indeed been applied in different forms, context and devices, but they are usually not considered as the main heat dissipation mechanism, or they have a different application. For instance, dimples in [14], have been used with fins; the mechanic of the working fluid is therefore different, as it aims at improving the effectiveness, adding complications into the HE.

The intended outcome of the proposed design is to remove the above-mentioned complications to create a cheaper and more aerodynamic solution, suitable for the emerging EV requirements. Such proposed simple layout is presented in Fig. 1.

Traditional HEs work through a principle of extension of a dissipative surface to facilitate the dissipation of heat. In the present layout, the concept of surface extension has been moved from the usual fins to a different topology of the shells, showing a dimpled pattern. The surface is designed to create vortices inside the cavities, creating a fluid path able to carry out the requested heat, literally using the fissures as a source of cold air supplied by the recirculation motions taking place in the channel. The characteristic dimensions of the proposed device are provided in Fig. 2.

Such device is attractive because of its potential for reducing production costs. Being symmetric and without fins, this HE allows a relatively cheap production procedure. In addition, it is designed to have a lower weight/volume ratio than traditional HE as it does not need either reservoir or fin schemes, bringing the porosity value (ratio of empty volume to total volume in a porous medium) of the designed device at 64.5% while a commercial solution usually reaches a value of the order of 53% [8].

2.1. Dynamic characterization

The dynamic analysis consists of a parametric study, carried out by

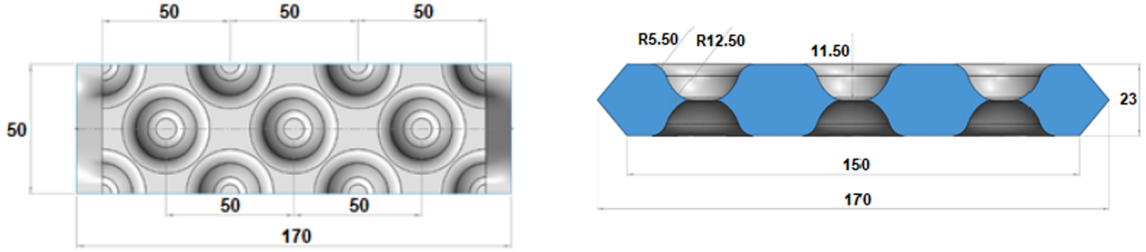


Fig. 2. HE's characteristic dimensions (mm).

testing the device under four different velocity conditions, using CFD to predict the pressure drop along the HE as a result of the vehicle movement. The virtual domain tests the airflow through a portion of the HE to make the simulation computationally manageable, based on the practices presented in [8], which scale the properties (thermal and dynamic) of a portion of the device to the whole system. The points of the parametric study are chosen by studying the vehicles' speed distribution on highways [15], an environment in which road EVs express the most dissipative phenomena. By setting 40 m/s as the point of maximum speed, equivalent to a velocity cumulative probability distribution of 99.95%, all the situations in which EV roads exhibit the highest dissipative phenomena are considered. These velocity values have been set at the inlet section of the domain (velocity-inlet type boundary condition), while a zero-pressure condition was applied at the outlet section (pressure outlet boundary condition). A wall-type boundary condition was considered for all hard surfaces of the HE. Simulating turbulence effects require a turbulence model implementation. Among the Reynolds Average Navier-Stokes (RANS) models, the *k-ω SST* turbulence model, identified from the literature [6], appears suitable for this study. The turbulent initial conditions have been described with a turbulence intensity set at 10%, with a 0.05 m characteristic length of the problem (distance between the HE's shells) [16]. The *SimpleFoam* with the *SIMPLEC* algorithm, which is a segregated, incompressible, and steady-state solver, is used to perform the simulations; it follows the following set of equations:

$$\nu_t = \frac{a_1 k}{\max(a_1\omega, SF_2)} \tag{1}$$

$$div(\vec{u}) = 0 \tag{2}$$

$$div(\vec{u}*\vec{u}) = -\frac{1}{\rho}\nabla \mathbf{p} + (\nu + \nu_t)\nabla^2\vec{u} + S_i \tag{3}$$

$$\mathbf{u_j}\frac{\partial \mathbf{k}}{\partial \mathbf{x_j}} = \frac{\partial}{\partial \mathbf{x_j}}\left[(\nu + \sigma_\mathbf{k}\nu_\mathbf{t})\frac{\partial \mathbf{k}}{\partial \mathbf{x_j}}\right] + \mathbf{P_k} - \beta^*\mathbf{k}\omega \quad \textbf{with} \quad \mathbf{j} = 1,2,3 \tag{4}$$

$$u_j\frac{\partial \omega}{\partial x_j} = \frac{\partial}{\partial x_j}\left[(\nu + \sigma_\omega\nu_t)\frac{\partial \omega}{\partial x_j}\right] + \alpha\rho S^2 - \beta\rho\omega^2 + 2(1-F_1)\sigma_{\omega 2}\frac{1}{\omega}\frac{\partial k}{\partial x_j}\frac{\partial \omega}{\partial x_j} \quad with \quad j = 1,2,3 \tag{5}$$

Equation (1) represents the Kinematic Eddy Viscosity (ν_t) formulation, Equation (2) is the Continuity equation, Equation (3) describes the Momentum equations, Equation (4) deals with the Turbulent Kinetic Energy (k) and Equation (5) describes the Specific Dissipation Rate (ω). The velocity vector is represented by u, the density by ρ, the kinematic viscosity by ν and the source terms by S_i, while S is the invariant measure of the strain rate. F_1, F_2, P_k are blending functions defined in [17]. Constants α, β, σ_k, σ_ω are computed by a blend from the corresponding constants via $\alpha = \alpha_1 F_1 + \alpha_2(1 - F_1)$, etc. The constants used in Equations (4) and (5) are therefore: $\alpha_1 = 5/9$, $\beta_1 = 3/40$, $\sigma_{k1} = 0.85$, $\sigma_{\omega 1} = 0.5$, $\alpha_2 = 0.44$, $\beta_2 = 0.0828$, $\sigma_{k2} = 1$, $\sigma_{\omega 2} = 0.856$, β^*=0.09, and $a_1 = 0.31$, see [17] for more details. Furthermore, these numerical settings have been chosen to remain aligned with the computational criteria found in [6], where a 1st order of discretization for the momentum, k, and ω equations have been applied in the discretization procedure. Wall functions have been selected for two reasons. The first one is that they allowed a coarser mesh to be generated at the wall, thus reducing the computational time and resources to get the results. The second reason is that the work presented here aimed at showing the advantages of using a new type of heat exchanger, not to have the most accurate results at this stage of the research. A finer grid at the wall will be however considered in future work, and other turbulence models will also be considered to obtain a higher accuracy of the results in this region.

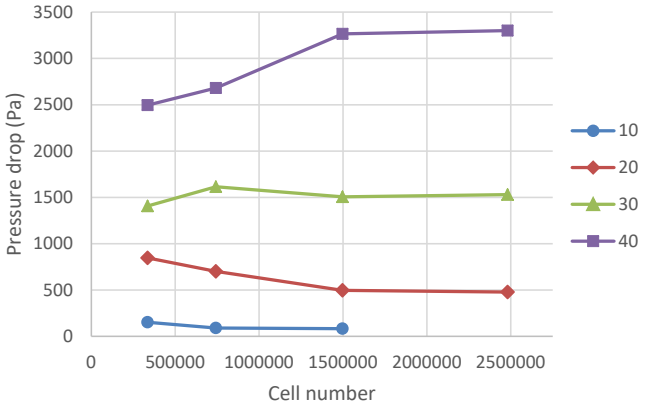


Fig. 3. Mesh independence study for the HE dynamic analysis.

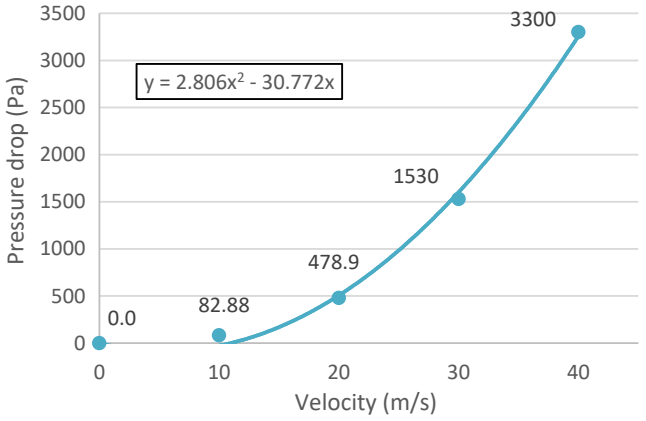


Fig. 4. Pressure drop chart.

Fig. 3 shows the outcomes of the mesh independence study performed for different inlet velocities ranging from 10 to 40 m/s. The investigation with 10 m/s shows mesh-independent results with a grid comprising around 7.5 × 10^5 cells. When increasing the velocity, convergence of the pressure drop is obtained with a more refined mesh, and results become mesh-independent with a mesh comprising 1.5 × 10^6 cells. Increasing the number of cells in the mesh does not show any difference in the results, this mesh has therefore been selected to generate the final outcomes.

Fig. 4 shows the aerodynamic performance of the device, with the pressure drop plotted against the inlet velocity. A best-fit equation can be generated from these results, described through the dashed line. As can be seen, the equation matches numerical results perfectly well if used for velocities higher than 20 m/s.

This best-fit relation is useful to characterise the HE as a porous body, to limit the computational effort in complicated computational models. This relation can indeed characterise the dynamic behaviour of the HE in the actual vehicle simulation. The standard adopted for this purpose is the Darcy-Forchheimer model [18], which is based on the pressure drop as a 2nd order polynomial function of the velocity, expressed through Equation (6).

$$\Delta Pa = Au^2 - Bu \tag{6}$$

Table 1
HE's Darcy-Forchheimer coefficients.

A	*2.806*
B	*30.772*

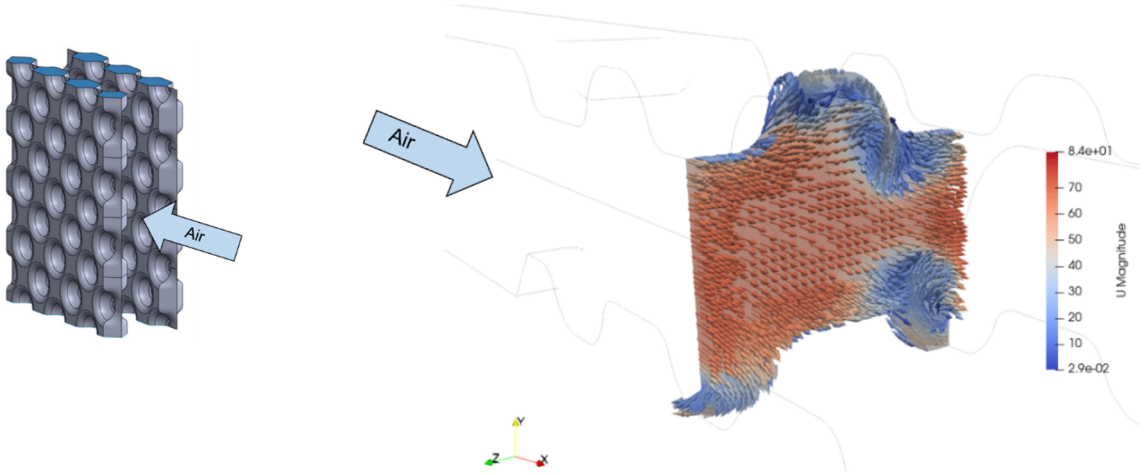


Fig. 5. Velocity field in HE cross-section [m/s] – Inlet velocity: 30 m/s.

where ΔPa is the pressure drop, u is the upstream velocity, A and B are coefficients deduced from the 2nd order polynomial function relating pressure drop to velocity. In this work, u it is assumed the same as the inlet of the fluid domain, A and B are approximated with the best fit equation from Fig. 4, their values are given in Table 1.

Regarding qualitative considerations of the fluid behaviour, peculiar phenomena are highlighted in Fig. 5, where the swirl effect is visible and a zero velocity is registered at the centre of the cavities, creating a non-zero velocity field along the dimples' hot surface.

2.2. Thermal characterization

The thermal characterisation takes place to quantify the heat transfer coefficient (h_c) which allows the HE to be dimensioned, given the vehicle's operational conditions. The h_c value is determined through CFD analysis, considering the average value of the HE surfaces, while the other parameters needed to set the boundary conditions of the problem, are deduced from the operational conditions of the vehicle. The computational domain considered here is slightly different from the one used in the dynamic analysis detailed in the previous section. The domain has thus been extended to avoid boundary effects at the outlet, but the HE portion considered for the evaluation of both the dynamic and the thermal analysis is identical. The thermal study has been performed using the OpenFOAM® *buoyantSimpleFoam* solver with a *SIMPLEC* scheme, which is a segregated, incompressible, and steady-state solver with heat transfer. An additional equation is therefore used to describe the thermal behaviour of the fluid:

$$\boldsymbol{div}(\rho\vec{\boldsymbol{u}}\boldsymbol{h}) + \boldsymbol{div}(\rho\vec{\boldsymbol{u}}\boldsymbol{K}) = \boldsymbol{div}\left(\boldsymbol{\alpha}_{\boldsymbol{eff}}\nabla\boldsymbol{h}\right) + \rho\vec{\boldsymbol{u}}\bullet\vec{\boldsymbol{g}} \tag{7}$$

where h is the enthalpy, K the kinetic energy per unit mass, u the velocity vector, ρ the density, g the gravitational acceleration, and α_{eff} the effective thermal diffusivity. As the velocity conditions require knowing the characteristics of the vehicle, its specifications and the dimensions of the HE a priori, a sensible guess of the velocity field must be done when using this solver. For the dynamic analysis, 40 m/s has thus been considered as the upper limit of velocity for the EV; this value is aimed for the HE to represent the heavy-duty of the vehicle. Note that even if the velocity of the vehicle itself is known in advance, it does not allow to infer the velocity in front of the HE since the frontal area of the HE remains unknown if the vehicle characteristics are unknown.

As there is a need to dimension the HE to perform a CFD analysis, a reference vehicle needs to be selected. The authors' choice has been towards a commercial sports car for which thermal/electric propulsion is currently being developed. This choice has also been dictated by this vehicle's available space to host HEs. Based on the characteristics of this car, the ratio between the duct inlet surface and the HE's frontal area is estimated around 50%. Consequently, an inlet velocity of 20 m/s has been selected to conduct the fluid flow analysis.

The wall temperature is estimated, based on two assumptions. First, because of the high thermal conductivity of the material considered here (aluminium), the HE wall temperature is considered constant along the surface. The second and strongest assumption is that the temperature value is assumed to be steady-state as the temperature is supposed to remain as high as possible from the heat management system, to enhance the enthalpy h. The physical limit of the working fluid (water without additives) inside the HE is the boiling point, which is 114.4 °C at a pressure of 1.5 bar (usual pressure limit inside an automotive cooling system). A reasonable safety factor is settled to 84% of this temperature, hence the considered temperature at the wall is set to 95.6 °C. No local phase transition was considered in this work. The atmospheric air temperature is considered at 25 °C. An under-relaxation factor of 0.3 is applied for the energy equation. All other boundary conditions and numerical setup remain identical to the dynamic analysis settings discussed previously in Section 2.1. The value of y^+, which is a dimensionless parameter that describes the distance of the first cell at the walls, is kept less than 3 during the analysis, following the advice provided in [19].

An initial mesh independence study carried out on h_c, has shown strong instabilities when the first cell height is very close to the wall (low y^+ value). This can be explained by the mesh refinement which has not

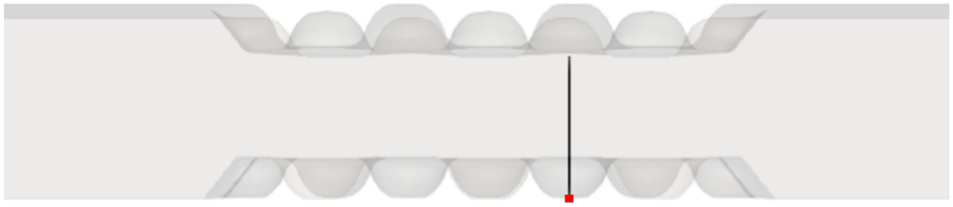


Fig. 6. Sampling line.

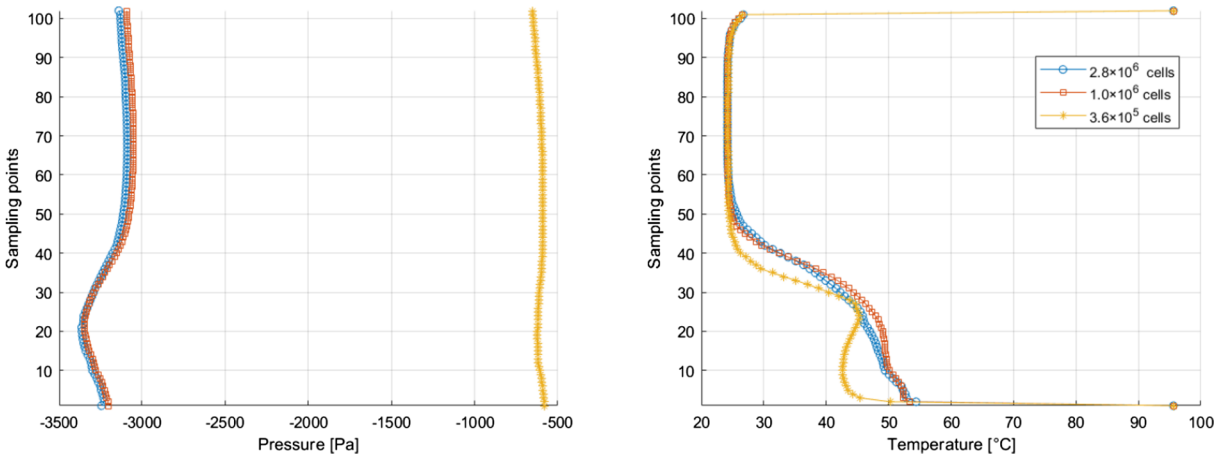


Fig. 7. Mesh independence study on pressure and temperature.

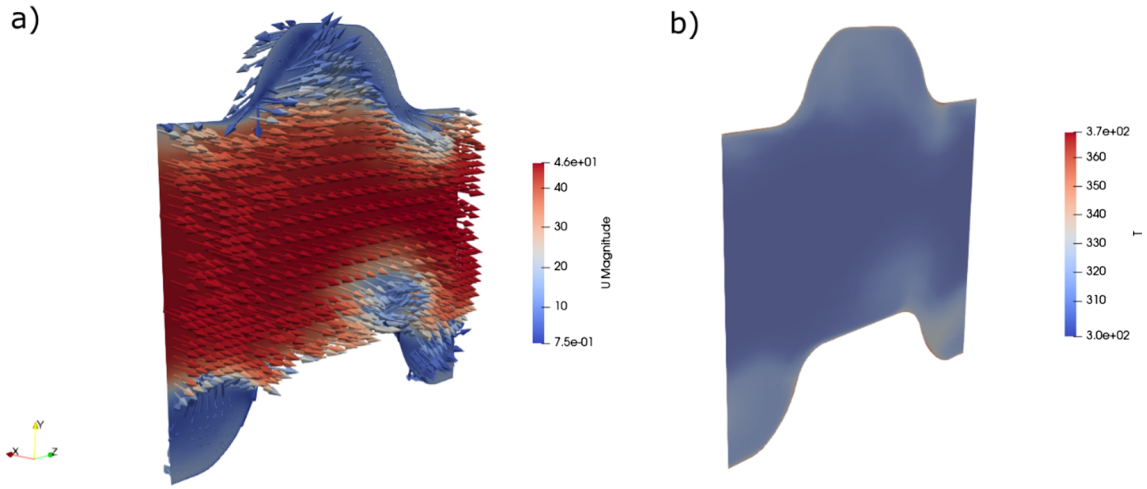


Fig. 8. Crosse-sectional view a) Velocity field [m/s], b) Temperature field [K].

been applied uniformly by the mesh generator throughout the entire boundary layer, leaving relatively large grid spaces in the presence of strong gradients. Note that h_c can anyway fail to capture a realistic temperature gradient since its formulation is reliant on a space definition function of the mesh, which might overestimate its value. The finest mesh of 3.5×10^6 cells thus, cannot be used to establish the h_c values, the results being considered unreliable. However, a suitable mesh has been established, following mesh independence studies for different variables (pressure and temperature) at a specific position of the HE, where the flow is established, see Fig. 6.

Fig. 7 shows the results of the mesh independence study, where pressure and temperature values are extracted along the sampling line shown in Fig. 6. Note that Sampling point 0 is located at the bottom of the HE, coincident with the shell of the HE, as indicated by the square pointer in Fig. 6. As can be seen in Fig. 7 the mesh comprising 1.0×10^6 cells and the one comprising 2.8×10^6 cells are considered suitable, as

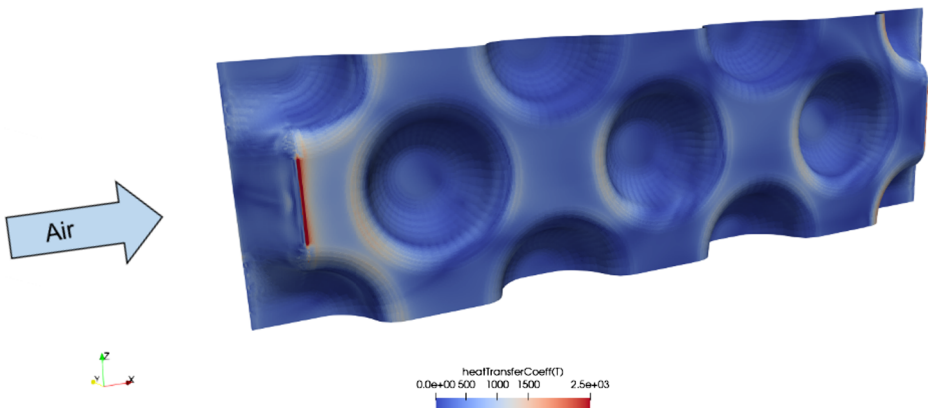


Fig. 9. Heat Transfer Coefficient (h_c) contours on the HE shell.

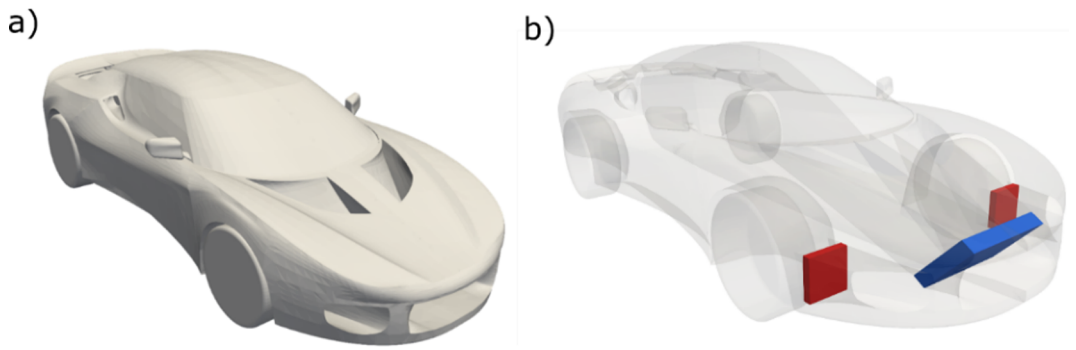


Fig. 10. 'Base' case model: a) Plain geometry b) Transparent view showing the HEs.

convergence is achieved. Ideally, the coarser of the two meshes should be selected to save time and computing resources. The finer one has nevertheless been selected here as it is expected that h_c results are more accurate with this mesh, and little time is added to the computation when using this mesh. A h_c value equal to 1209 W/m^{2}K obtained with the finer mesh is thus assumed reliable, as both pressure and temperature are shown to be mesh independent.

The thermal requirement of the car, retrieved from a proprietary commercial source, is up to 55 KW. Consequently, the amount of dissipative surface needed to cover this vehicle thermal load has been derived using Equation (8).

$$\boldsymbol{W = h_c A(T_{HE} - T_{air})} \tag{8}$$

where W is the power to dissipate, A the surface where the heat transfer is studied, T_{HE} the temperature of the HE' shells and T_{air} the temperature taken far from the walls, set as the inlet temperature condition. Note that this proposed HE design is probably less effective than traditional HEs, as larger volumes of free space are required to achieve sufficient performance to meet its primary task. However, the resulting dissipative surface still makes this device suitable for automotive applications in this type of vehicle. At this stage, a comparison with commercial HE solutions is however highly difficult as such data is usually proprietary and thus not available from the open literature.

The velocity distribution and the thermal features obtained with the final selected mesh are shown in Fig. 8. Vorticose patterns inside the cavities provide cold air from the internal regions of the channel to the exchange surfaces, enhancing heat flux. The vorticity zones create a zero-velocity region in the centre of the dimples as shown in Fig. 8a, allowing the fluid to recirculate quickly near the shell, and thus transporting the heat in a vorticose pattern which brings the warmed air to the centre of the channel, see Fig. 8b.

To better understand the impact of the HE shell on the temperature distribution in the system, the heat transfer coefficient h_c is provided in Fig. 9. As can be seen, h_c values are maximum at the entrance of the system, and decrease as air progresses, due to the presence of the dimples. The h_c values are thus the lowest on the walls of these dimples, near regions where the flow recirculation is maximum.

3. Real case scenario

To understand and evaluate the dynamic impact that the developed HE has on the vehicle, two different systems of the vehicle internal body are created to assess the aerodynamic performance and the mass flow delivered to the radiating parts. The objective is now to establish how the proposed HE along with specific vehicle internal design criteria can provide quantitative information for potential future development/evolution of current vehicles.

A model representing a current vehicle, denoted 'Base' case, is built first. To better meet EV requirements, a redesigned HE is then considered, and the second computational model is denoted 'New' case. The latter case thus requires major modifications of the former one. To model the HEs contained in these domains, porous bodies have been considered, described by the Darcy-Forchheimer formulation in Equation (6) [2021].

Table 2
Porosity value for the 'base' case.

Component	Colour	Darcy-Forchheimer model
Central HE	Red	$\Delta Pa = 12.079u^2 + 51.479u$
Lateral HE	Blue	$\Delta Pa = 5.192u^2 + 22.346u$

For the 'Base' case study, all the cooling units in the vehicle have been concentrated in two clusters of radiators to allow a straightforward model build-up, which includes the HEs of the vehicle. These clusters are shown in Fig. 10b, with red and blue colours highlighting the different permeability levels. These permeability levels have been retrieved from proprietary experimental data and are defined through the Darcy-Forchheimer formulation summarised in Table 2, for direct comparison with Table 1.

To enable the implementation of the proposed HE in a BEV, new design criteria are also introduced, which consist in relocating the cooling units to the rear part of the car. A positioning different from the standard one is recommended, since the reduced dissipative capacity of the new HE requires a larger volume to meet the thermal requirement of the vehicle; this makes the proposed device unsuitable for the front position of the car. It is thus advised that manufacturers select a vehicle layout similar to the one displayed in Fig. 11 ('New' case), to enable a thermal/electrical transition of the powertrain when coupled with the proposed HE.

To describe further the new configuration of the car in Fig. 11, the main HEs have been dimensioned and positioned at the back end of the car (within two symmetrical ducts specifically sized to accommodate them), to cover the new thermal load of the vehicle (blue coloured). Two pre-installed units at the front end of the car (red coloured) have however been left in place to enable additional thermal systems at the front location of the vehicle for auxiliary systems, such as air conditioning.

The details of these ducts and their position at the vehicle's back end are shown in Fig. 12a and Fig. 12b.

The CFD simulations of the external flow are based on the *porousSimpleFoam* solver with a *SIMPLEC* scheme, which is a segregated, incompressible, and steady-state solver with porous body implementation. This solver uses Equations (1)-(5), setting the source term S_i as:

$$\boldsymbol{S_i = \frac{1}{\rho}(A|\vec{u}|\vec{u} + B\vec{u})} \tag{9}$$

where $\vec{u}$ is the velocity vector, and ρ the density. A and B are constants, extrapolated from the Darcy-Forchheimer formulation (c.f. Table 1). The computational domain includes the car body shape and is delimited by boundaries located far enough from the car, so that they do not influence

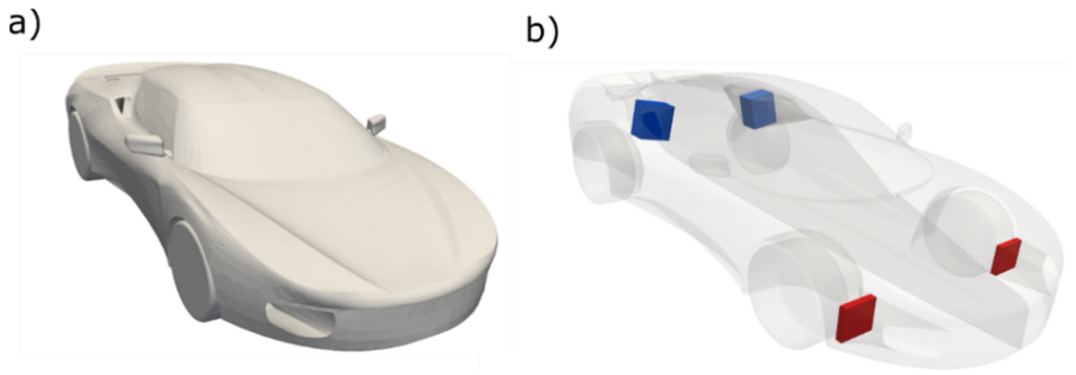


Fig. 11. 'New' case model: a) Plain Geometry b) Transparent view to locate HEs.

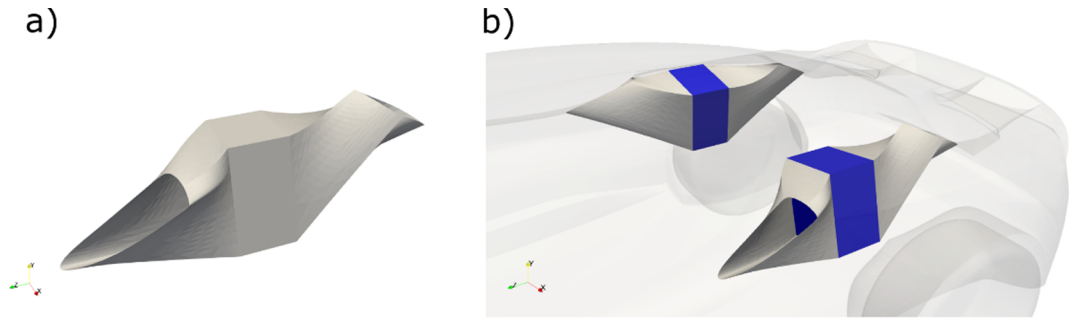


Fig. 12. Rear ducts: a) Single duct view b) Rear positioning of the HEs.

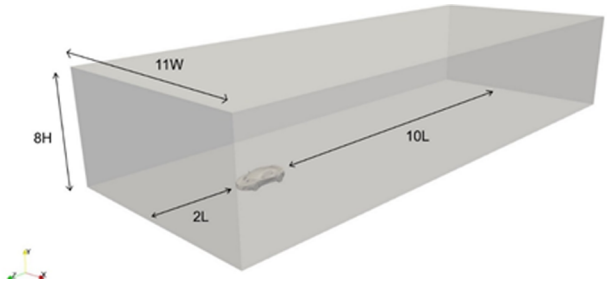


Fig. 13. Computational domain.

Table 3
Vehicle's dimensions.

Property	Abbreviation	Value	Unit
Length	L	4.342	m
Height	H	1.223	m
Width	W	1.848	m
Frontal area	A_{ref}	1.85	m^2

the flow field in the region of interest (vicinity of the car), see Fig. 13. Fluid domain boundaries lengths are extracted from [20]. The height, width and length considered here are 13 L, 8H, and 11 W, with L, H and W the length, width, and height of the vehicle, respectively, as reported in Table 3.

The actual car body is positioned 2L far from the inlet. Note that although Fig. 13 shows the full computational model, to simplify the model and save computing and power resources, half the car and domain has been simulated, and a symmetry boundary condition applied.

The velocity at the inlet section of the domain has been chosen as 40 m/s to recreate standard conditions in which the force coefficients are usually calculated [20]–[23], this corresponds to a Reynolds number $Re = uL/\nu = 11.6 \times 10^6$ with u is the fluid velocity at the inlet of the domain, L the vehicle length and ν the kinematic viscosity. A zero-pressure condition is applied at the outlet section of the domain. No recirculation effects are expected far away from the vehicle; hence no velocity constrain at the outlet boundary is considered. A no-slip boundary condition is enforced for the geometry of the car itself while for the ground, a moving wall is considered, with a velocity equal to the inlet velocity. A slip boundary condition is chosen for the sidewalls and the top of the domain, although a symmetry type boundary condition could have been applied. As mentioned previously, as those boundaries are far away from the car, they will not influence the flow field in the near-car region. The *RANS k-ω-SST* turbulence model is considered, with wall-functions, as specified previously. Although more accurate models for automotive applications are commonly applied, such as Detached Eddy Simulation (DES) variants, they are considered excessively onerous regarding computational cost [2324]. The turbulent intensity is set to 1% and the turbulent viscosity ratio is equal to 10, following the recommendations provided in [22]. The simulation has been carried out with a 2nd order discretization on momentum, turbulence kinetic energy k and specific rate of dissipation ω. Under-relaxation factors of 0.3 for pressure and 0.7 for momentum, k, and ω were applied.

Note that the addition of new vehicle design criteria is justified by the lower incident mass flow rate at the rear of the vehicle which allows the proposed HEs to be placed at the locations depicted in Fig. 11b due to their high permeability (c.f. Table 1 and Table 2), allowing an adequate air flow through the duct. The guarantee that the mass flow rate is sufficient is provided through a mapping of the boundary conditions used in the thermal study (c.f. Section 2.2) with the flow conditions within the rear ducts in the whole vehicle-based computational model. Given that the size of the HE is based on h_C (velocity field dependent parameter), and is estimated for an inlet velocity of 20 m/s, the size of the ducts in the 'New' model-based vehicle has therefore been evaluated to comply with the velocity required for the devices to show the same thermal properties as discussed previously in Section 2.2. Subsequently,



Fig. 14. Vehicle Frontal Area.

the external flow field for the entire vehicle for which 40 m/s has been applied at the inlet of the computational domain, has been established to provide an average magnitude around 20 m/s upstream of the HEs, reproducing the conditions under which the h_C has been tested in Section 2.2, and demonstrating that the proposed HEs are able to sustain the thermal load of the vehicle in the conditions for which they have been designed.

The force coefficients of the vehicle are calculated, coefficients of drag (C_D) and lift (C_L), which respectively give an estimate of the forces acting in the opposite direction of travel and towards the ground:

$$C_D = \frac{1}{2}\frac{\oiint_{car} F_z}{\rho U^2 A_{ref}} \tag{10}$$

$$C_L = \frac{1}{2}\frac{\oiint_{car} F_y}{\rho U^2 A_{ref}} \tag{11}$$

where F is the infinitesimal force acting on the surface of the vehicle according to the reference system in Fig. 14, U is the vehicle velocity, A_{ref} is the frontal area of the car as provided in Table 3, and ρ is the density of air. Furthermore, an estimation of the drag contribution is given for the cooling units, providing the force coefficient $C_{D\ POROUS}$:

$$C_{D\ POROUS} = \frac{1}{2}\frac{\odot\iiint_{HE} F_z}{\rho U^2 A_{ref}} \tag{12}$$

where F is the infinitesimal force acting on the volume of the HE, according to the reference frame in Fig. 14.

A mesh independence study has also been performed on C_D for both 'base' and 'new' cases; the corresponding results are displayed in Fig. 15.

Mesh independent results are obtained with a mesh comprising 7×10^6 cells, which has therefore been selected for this study. The benefits of increasing the mesh density are marginal while increasing the computational cost of the simulations.

The corresponding CFD results obtained with the 7×10^6 cells mesh, are summarised in Fig. 16. It is estimated that a reduction of C_D and C_L of approximately 5% and 21% respectively, is obtained when the 'new' HE is installed. '$C_{D\ POROUS}$' in Fig. 16 denotes the contribution of the drag produced by the porous body present in the domain. The influence of the cooling units during the motion of the vehicle can thus be deduced.

As can be seen, both C_D and C_L have been reduced with the "New" model, this can be explained by the removal of the central/frontal duct, deemed to generate downforce due to its inclination, and also by the permeability reduction of the proposed HE, returning force coefficients more suitable for a BEV. It is retained that the reduction of C_D is primarily caused by the implementation of more permeable cooling units, while the reduction of C_L is mainly due to the removal of the frontal duct.

A reduction of C_D is always welcome by car designers, but a reduction of C_L must be compensated by a force weight. However, if the vehicle changes its powertrain type, inevitably, the added weight from the addition of a battery pack will make the "New model" a suitable design option.

Results from the literature show an indicative discrepancy between values obtained from CFD simulations and those obtained from experimental data around 2.6% with a mesh comprising 40×10^6 cells, and around 4.3% with a mesh comprising 20×10^6 cells, for a similar vehicle shape without implementation of wall functions [25]. In the work described here, the mesh was built for applying wall functions, this offers the advantage of limiting the number of cells in the domain. However, the use of wall functions also induces larger numerical discrepancies at the wall. The current simulations have therefore been affected, and the comparison of the base model with the respective

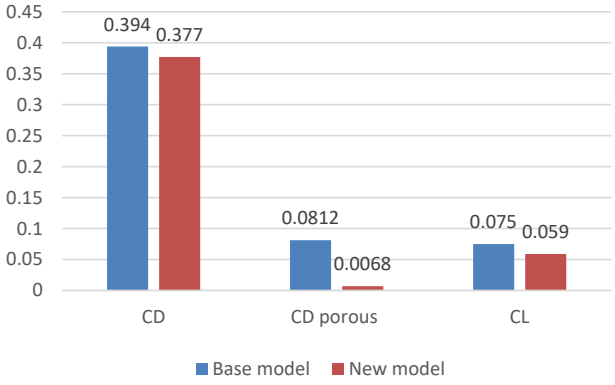


Fig. 16. Comparison between the different aerodynamic coefficients of drag, drag porous, and lift for the 'base' and 'new' models.

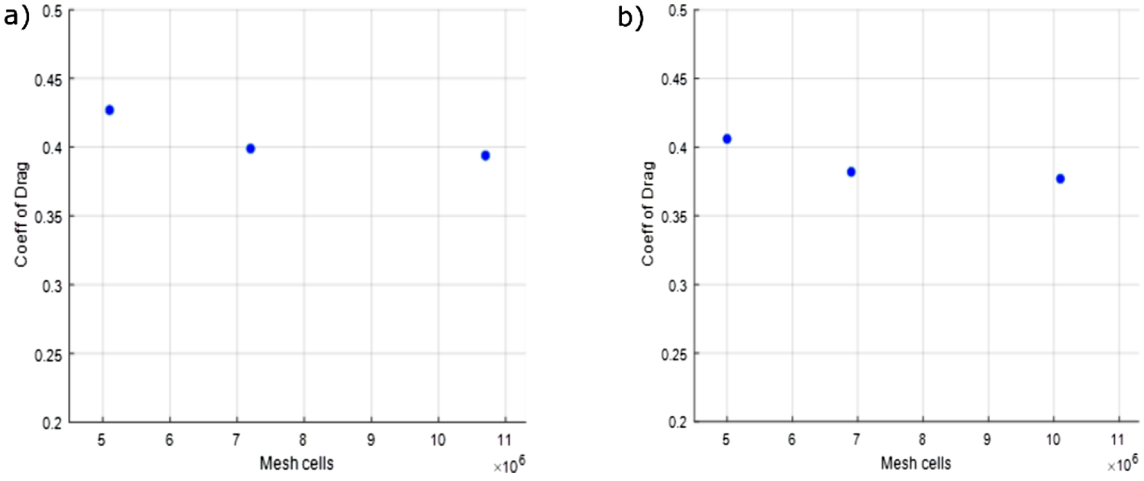


Fig. 15. Mesh independence study on C_D: a) 'base' case b) 'new' case.

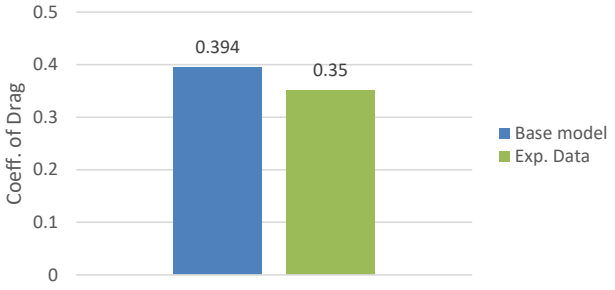


Fig. 17. Experimental data comparison.

proprietary experimental data is provided in Fig. 17, showing an error of about 12.6%. This error might also be explained by the geometry simplification adopted in this work when compared to the 'real' vehicle shape.

The model simplifications from the design procedure (CAD geometry) and choice of turbulence model therefore seem acceptable for this study. At this stage, however, it appears difficult to quantify the error coming from the use of wall functions in the turbulence formulation, and the error coming from the difference of design geometry. However, these two points have been identified as the major causes of the discrepancies with the experimental data, and further investigations are needed to refine the mesh in the near-wall region, and consider a different turbulence model, to establish more precisely the effects due to the use of wall functions.

4. Conclusions

A new concept has been proposed for the heat exchange mechanism inside electrical vehicles HEs. A procedure has been described to carry out a numerical study, from the first sketch until the first phase of prototyping, providing the necessary numerical data to justify the building of a physical model. Further work is however required for the creation and optimization of the prototype through experimental studies. Additional CFD studies should also be performed to quantify better the error due to the simplification of the design, and the error due to the wall treatment and choice of turbulence model on the aerodynamic coefficients of the vehicle.

This initial study has provided meaningful data for installing the designed cooling units, showing that a reduction of 5% on the coefficient of drag can be achieved relative to its thermal counterpart. As discussed, the proposed design is expected to be cheaper and lighter than traditional ones. Experimental validation and optimization procedures should also take place, to check and confirm the feasibility of using the proposed device for electric sports vehicles.

Declaration of Competing Interest

The authors declare that they have no known competing financial interests or personal relationships that could have appeared to influence the work reported in this paper.

References

[1] J.P. Yadav, B.R. Singh, Study on performance evaluation of automotive radiator, SAMRIDDHI A J. Phys. Sci. Eng. Technol. 2 (2) (2015) 47–56, https://doi.org/10.18090/samriddhi.v2i2.1604.
[2] F.W. Geels, A socio-technical analysis of low-carbon transitions: introducing the multi-level perspective into transport studies, J. Transp. Geogr. 24 (2012) 471–482, https://doi.org/10.1016/j.jtrangeo.2012.01.021.
[3] C. Oliet, A. Oliva, J. Castro, C.D. Pérez-Segarra, Parametric studies on automotive radiators, Appl. Therm. Eng. 27 (11–12) (2007) 2033–2043, https://doi.org/10.1016/j.applthermaleng.2006.12.006.
[4] D. Antonijevic, An engineering procedure for air side performance evaluation of flat tube heat exchangers with louvered fins, Heat Mass Transf. und Stoffuebertragung 49 (1) (2013) 117–127, https://doi.org/10.1007/s00231-012-1073-z.
[5] F.N. Beauvais, An aerodynamic look at automotive radiators, SAE Tech. Pap. (1965), https://doi.org/10.4271/650470.
[6] G.C. Junjanna, N. Kulasekharan, H.R. Purushotham, Performance improvement of a louver-finned automobile radiator using conjugate thermal CFD analysis, Int. J. Eng. Res. Technol. 1 (8) (2012) 1–13.
[7] R. Kahraman, D. Bacheva, A. Schmieder, G.R. Tabor, Coupling of volume of fluid and level set methods in condensing heat transfer simulations, Int. J. Comut. Fluid Dyn. 34 (1) (2020) 25–38, https://doi.org/10.1080/10618562.2019.1693546.
[8] B. Çetin, K.G. Güler, M.H. Aksel, Computational modeling of vehicle radiators using porous medium approach, Heat Exch. - Des. Exp. Simul. (2017), https://doi.org/10.5772/66281.
[9] R.K. Shah, D.P. Sekulic, Fundamentals of heat exchanger design, Wiley, 2003.
[10] S. Ramalingam, R. Dhairiyasamy, M. Govindasamy, Assessment of heat transfer characteristics and system physiognomies using hybrid nanofluids in an automotive radiator, Chem. Eng. Process. - Process Intensification 150 (2020) 107886.
[11] M.H. Salah, T.H. Mitchell, J.R. Wagner, D.M. Dawson, A smart multiple-loop automotive cooling system-model, control, and experimental study, IEEE/ASME Trans. Mechatronics 15 (1) (2010) 117–124, https://doi.org/10.1109/TMECH.2009.2019723.
[12] A.I. Heft, T. Indinger, N.A. Adams, Experimental and numerical investigation of the drivaer model, in American Society of Mechanical Engineers, Fluids Engineering Division (Publication) FEDSM, 2012, vol. 1, no. PARTS A AND B, pp. 41–51, doi: 10.1115/FEDSM2012-72272.
[13] T. Marić, J. Höpken, K. G. Mooney, The OpenFOAM technology primer, 2014.
[14] E.M. Sparrow, J.M. Gorman, K.S. Friend, J.P. Abraham, Flow regime determination for finned heat exchanger surfaces with dimples/protrusions, Numer. Heat Transf. Part A Appl. 63 (4) (2013) 245–256, https://doi.org/10.1080/10407782.2013.730450.
[15] "Vehicle Speed Compliance Statistics". www.gov.uk (2019).
[16] "OpenFOAM: User Guide v2012." www.openfoam.com.
[17] F.R. Menter, M. Kuntz, R. Langtry, in: Ten Years of Industrial Experience with the SST Turbulence Model, Begell House Inc., West Redding, 2003, pp. 625–632.
[18] S. Whitaker, Flow in porous media I: A theoretical derivation of Darcy's law, Transp. Porous Media 1 (1) (1986) 3–25, https://doi.org/10.1007/BF01036523.
[19] F.R. Menter, Two-equation eddy-viscosity turbulence models for engineering applications, AIAA J. 32 (8) (1994) 1598–1605, https://doi.org/10.2514/3.12149.
[20] E. Guilmineau, Numerical simulations of flow around a realistic generic car model, SAE Int J. Passeng. Cars - Mech. Syst. 7 (2) (2014) 646–653, https://doi.org/10.4271/2014-01-0607.
[21] S. Mansor, N.A.R. Nik Mohd, C.W. Chung, CFD simulation of a simplified automotive model for various rear slant angle, Appl. Mech. Mater. 660 (October) (2014) 724–729, https://doi.org/10.4028/www.scientific.net/AMM.660.724.
[22] N. Ashton, A. West, S. Lardeau, A. Revell, Assessment of RANS and DES methods for realistic automotive models, Comput. Fluids 128 (2016) 1–15, https://doi.org/10.1016/j.compfluid.2016.01.008.
[23] E. Guilmineau, G.B. Deng, J. Wackers, Numerical simulation with a DES approach for automotive flows, J. Fluids Struct. 27 (5–6) (2011) 807–816, https://doi.org/10.1016/j.jfluidstructs.2011.03.010.
[24] R.J.A. Howard, M. Pourquie, Large eddy simulation of an Ahmed reference model, J. Turbul. 3 (April) (2016) 2002, https://doi.org/10.1088/1468-5248/3/1/012.
[25] J. Cho, J. Park, K. Yee, H.L. Kim, Comparison of various drag reduction devices and their aerodynamic effects on the DrivAer model, SAE Int. J. Passeng. Cars - Mech. Syst. 11 (3) (2018) 225–237, https://doi.org/10.4271/06-11-03-0019.



https://dspace.org/

Numerical modelling of a finless heat exchanger layout for electric vehicle application

Samiolo, Mattia; Verdin, Patrick G.

2022-04-11
Elsevier
https://doi.org/10.1016/j.applthermaleng.2022.118506
Samiolo M, Verdin PG. (2022) Numerical modelling of a finless heat exchanger layout for electric vehicle application. Applied Thermal Engineering, Volume 211, July 2022, Article number 118506

Downloaded from a DSpace repository. https://dspace.org/